

Article

Fault Tolerant Digital Datapath Design Via Control Feedback Loops

Oana Boncalo ^{1,†} , Alexandru Amaricai ^{1,†}  and Zsófia Lendek ^{2,*} 

¹ Universitatea Politehnica Timisoara; oana.boncalo@cs.upt.ro, alexandru.amaricai@cs.upt.ro

² Technical University of Cluj-Napoca; Zsofia.Lendek@aut.utcluj.ro

* Correspondence: oana.boncalo@cs.upt.ro; Tel.: +40-256-403264

† Address: Timisoara, Blvd. Vasile Parvan, Nr. 2

Version October 20, 2020 submitted to Electronics

Abstract: In this paper, we propose a novel fault tolerant methodology for digital pipelined data-paths called Control Feedback Loop Error Decimation (CFLED), that reduces the error magnitude at the outputs. The data-path is regarded from a control perspective as a process affected by perturbations or faults. Based on the corresponding dynamic model, we design feedback control loops with the goal of attenuating the effect of the faults on the output. The correction loops apply correction factors to selected data-path registers from blocks that have their execution rewinded. We apply the proposed methodology on the data-path of a controller designed for a 2-degree-of-freedom robot arm, and compare the cost and reliability to the generic triple modular redundancy. For FPGA technology, the solution we propose uses 30% less slices with respect to TMR, while having a third less DSP blocks. Simulation results show that our approach improves the reliability and error detection.

Keywords: Fault tolerance, reliability, arithmetic datapath, FPGA, control engineering, feedback controller

1. Introduction

Reliability represents a key factor in electronic devices that operate in radiation prone environments, frequent in applications in the aerospace domain. It is achieved by adding redundancy to the digital circuits, with cost increase acting as the main drawback. Fault tolerant design is based on adding some form of replication, or using specially designed error detection and correction codes, so that the cost overhead with respect to the nominal solution is acceptable, and the target reliability is achieved.

The most common way of increasing the reliability of a circuit is to employ Triple Modular Redundancy (TMR), i.e., using three copies of the digital circuit and a voter structure [1]. The main drawbacks of TMR are its high cost and the sensitivity of errors affecting the voters. Regarding the former, schemes to reduce the cost of the TMR, such as approximate TMR [2–4] or inexact TMR [5] have been proposed. Furthermore, the use of TMR in the context of approximate computing is discussed in [6]. For arithmetic circuits, the concept of reduced precision replicas has been applied, with the most significant part of the circuit being triplicated [7,8]. Reduced precision replicas can also be used in a dual manner, with the lower cost data-path working in a higher supply voltage domain and providing a highly reliable reference [9]. Other works improved reliability by increasing the resilience of the voting circuits within the TMR, such as the self checking voting circuits [10], adaptable bit-width voter [11], or employing dedicated voters for approximate TMR [12].

Modular redundancy approaches use multiple instances or truncated versions of the same nominal circuit. Other solutions use different types of redundancies. For example, approaches using error correction codes – Hamming or Reed-Muller codes – in combinational circuits have been proposed

in [13]. Redundant residue number systems have been employed for signal processing datapaths in [14,15]; in this case, modular redundancy is employed, with each replica having its own residue representation. Another approach uses a design inspired from the Markov Random Field (MRF) theory. In [16], a complementary dual modular redundancy with an MRF voter is proposed, while [17] uses coding based partial MRF, where the circuit is employed using MRF based logic components. The common drawback of MRF based implementations is the high implementation cost. Therefore, for non time-critical applications, several approaches using testing methods and redundancy have been proposed [18], with fault detection being performed during a circuit testing phase.

Different from all the mentioned approaches, this work proposes a control engineering approach – CFLED – for improving the reliability of digital data-path processing pipelines, by employing feedback control loops to reduce the error magnitude. CFLED targets applications that rely heavily on arithmetic operations, such as signal and image processing or control and artificial intelligence applications. In arithmetic data-paths, error magnitude is an important factor, as low-magnitude errors may be tolerated by the application. The goal of reducing the error magnitude, and not to completely remove the fault, is also employed in fault tolerant techniques that rely on approximate redundancy [2,4,6], inexact redundancy [5] or reduced precision replicas [8]. The proposed technique may be applied for arithmetic data-paths implemented on both ASIC and FPGA technology.

To the best of our knowledge, CFLED represents the first approach that uses control theory in order to improve the reliability of processing datapaths. Fault-tolerant control for finite state machines has been considered in e.g., [19,20]. The design for these use cases is aided by the finite state machine characteristics: finite and rather low (at most tens) number of states, low number of inputs (typically 1-bit inputs), and finite number of state transitions. In contrast, the proposed approach considers a dynamic model that captures high order input-state-output dynamics, where inputs, states and outputs have continuous values within their variation domains.

We analyzed the proposed approach on the hardware architecture for the two-degree of freedom robotic arm controller (2-DOF) presented in [21]. The considered use case consists of a processing pipeline that relies on function evaluations – performed using Taylor series –, scalar-matrix multiplications, and vector-matrix multiplications. Such operations are widely used in applications such as graphic processing and signal and image processing. Furthermore, this use case represents a novel application in control engineering: design of fault tolerant controller when the faults affect the controller implementation. Other approaches for fault-tolerant control, such the ones used for electronic power converters [22], induction motors [23], filters [24], robot control and localization [25,26], assume faults in components of the controlled system, usually actuators or sensors.

This paper is organized as follows: Section 2 discusses the methodology – the discrete time dynamical model of the circuit used to derive the feedback controller; Section 3 discusses a case study for the proposed methodology and presents FPGA implementation costs and reliability estimates; concluding remarks are presented in Section 4.

2. Control Feedback Loop for Fault Mitigation

The proposed methodology targets arithmetic data-path circuits consisting of several processing stages built out of arithmetic operations: additions, accumulations, multiplications and multiply-add fused. The operands can be either registers or constants. Thus, we consider data-paths commonly used in a wide variety of applications fields that rely on matrix-vector/matrix-matrix multiplications, convolutions, or weighted sums, and are therefore dominant in fields like signal and image processing, computer graphics, or artificial intelligence. Each processing stage i consists of a sequence of registers $\{R_0^i, R_1^i, \dots, R_{n_i}^i\}$, and it takes n_i clock cycles to compute a set of n_s^i data output elements out of a total of n_{el}^i data values stored to memory or inside registers. Thus, in order to produce a set of output results for stage i a total of $n_i \times \lceil n_{el}^i / n_s^i \rceil$ clock cycles (cc) are required.

81 The design process for enhancing the reliability of a given nominal circuit data-path involves:
 82 (i) Modeling the nominal circuit, (ii) CFLED design and simulation, (iii) CFLED operation, and (iv)
 83 Hardware implementation of the enhanced CFLED circuit.

84 2.1. Dynamic Model of Digital Datapath

85 Given a digital datapath, our first goal is to develop a mathematical model of the operations
 86 performed and the propagation of values through the datapath. This model forms the basis for
 87 designing a control law that will be used to correct the output of the circuit.

A common way to model a system from a control perspective is by using a state space representation. Since digital circuits are synchronous, we employ a discrete time-domain state-space representation, where the sample k corresponds to the current clock cycle, and has the general form:

$$x(k+1) = f(x(k), u(k), \eta) \quad (1)$$

88 where x denotes the states describing the circuit, u the inputs, η some parameters of the dynamic
 89 system, and f is a vector function – to be determined – that describes the evolution of the states in
 90 time. For a given circuit, each (partial) result (in case of iterative loops) is mapped to a state variable.
 91 Hence, each meaningful register value at different clock cycles has a corresponding state variable.
 92 Furthermore, a data-path (process) model is built by the composition of several processing stages i .

93 In this work we consider arithmetic data-path circuits, with the operations: addition,
 94 accumulation, multiplication and multiply-add. Since we map each (partial) result to a state, the
 95 value of the state may be obtained as either: 1) addition of a constant to a state; 2) addition of two
 96 states; 3) multiplication of a state by a constant; or 4) multiplication of two states. The dynamic model
 97 that describes the circuit aggregates all the operations throughout the clock cycles and therefore it may
 98 contain only these four mathematical operations. Consequently, the model chosen is of the form:

$$x(k+1) = Q\kappa(x(k)) + Ax(k) + a + \delta \quad (2)$$

99 where $\kappa(x(k))$ denotes the Kronecker product of the vector $x(k)$ with $x(k)$, Q and A are matrices of
 100 appropriate dimensions, a is the vector of biases or affine terms, and δ denotes the faults, possibly with
 101 a known distribution.

102 To determine the exact values of the parameters – matrices Q and A and affine term a – and the
 103 correspondence between the states and registers, we adopt the following convention:

- 104 1. The affine term a contains all inputs to the circuit.
- 105 2. Since scalar multiplications are commutative, the Q matrix is not unique. Nonzero values should
 106 appear in the first element corresponding to a multiplication.

107 The model and its parameters are obtained as follows:

- 108 1. Write the chronological operations for each clock cycle;
- 109 2. Assign a state variable to every register containing a partial result at different clock cycles;
- 110 3. Define the dynamic of each state variable as the operations performed to obtain the value in the
 111 corresponding register at the corresponding clock cycle;
- 112 4. Separate the bilinear, linear, and affine terms in the resulting equations;
- 113 5. Collect the coefficients of the bilinear terms in the matrix Q , the coefficients of the linear terms in
 114 the matrix A , while the affine terms, including the inputs to the data-path, will form the vector a .

115 Note that a model developed for a given circuit is not unique. We have formulated a generic
 116 dynamic structure that can be used for any circuit implementing arithmetic operations. In what follows,
 117 we illustrate the modeling steps on the circuit in Fig. 1.

In this example, In_1 and In_2 denote the inputs of the circuit. We define the state variables as the register values (states) in reverse order, i.e., $x_1(k+1) = R3(n+2)$, $x_2(k+1) = R2(n+1)$, etc., and

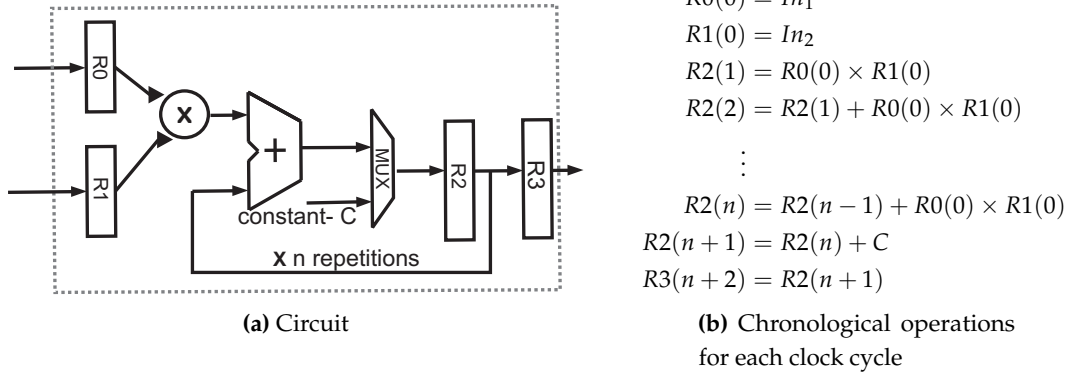


Figure 1. Modeling example: $R_i(m)$ denotes the value assigned to register R_i at the clock cycle m , and In_1 and In_2 are the MAC design unit inputs.

express each of them as a function of the state variables at the previous sample. This leads to the state equations:

$$\begin{aligned}
 x_{n+3}(k+1) &= In_1 \\
 x_{n+2}(k+1) &= In_2 \\
 x_{n+1}(k+1) &= x_{n+3}(k) \times x_{n+2}(k) \\
 x_n(k+1) &= x_{n+1}(k) + x_{n+3}(k) \times x_{n+2}(k) \\
 &\vdots \\
 x_3(k+1) &= x_4(k) + x_{n+3}(k) \times x_{n+2}(k) \\
 x_2(k+1) &= x_3(k) + C \\
 x_1(k+1) &= x_2(k)
 \end{aligned} \tag{3}$$

which can be written in a vector form as

$$\mathbf{x}(k+1) = Q\kappa(\mathbf{x}(k)) + A\mathbf{x} + a$$

118 where $Q = \begin{pmatrix} 0_{2 \times (n+3)^2} & & \\ 0_{(n-1) \times ((n+2)(n+3)-1)} & \mathbb{1}_{(n-1)} & 0_{n \times (n+3)} \\ & 0_{2 \times (n+3)^2} & \end{pmatrix}$, $A = \begin{pmatrix} 0_{n \times 1} & I_n & 0_{n \times 2} \\ 0_{n \times 1} & 0_n & 0_{n \times 2} \end{pmatrix}$, $a = \begin{pmatrix} 0 \\ C \\ 0_{(n-1) \times 1} \\ In_2 \\ In_1 \end{pmatrix}$,

119 with $0_{n \times m}$ we denote the zero matrix of dimensions $n \times m$, I_n the identity matrix, and $\mathbb{1}_n$ a column
120 vector of 1s.

121

122 Models of multiple pipelined sub-components can be combined as follows: (1) The outputs of
123 pipeline stage block i become states of pipeline stage $i+1$; (2) Modifying the matrices A and Q and
124 vector a appropriately. Thus, larger models of more complex circuits can be built from individual
125 sub-models of its parts.

126 2.2. Controller Design

The first objective of the controller is to reduce the fault effect at the digital circuit outputs, such that it is as close as possible to a reference value (*i.e.* gold output result). The second objective is to

converge as fast as possible to the correct value. A way to include control inputs into model (2) is to include a linear input, modifying the system model as

$$\begin{aligned} \mathbf{x}(k+1) &= Q\kappa(\mathbf{x}(k)) + A\mathbf{x}(k) + a + \delta + B\mathbf{u}(k) \\ \mathbf{y}(k) &= C\mathbf{x}(k) \end{aligned} \quad (4)$$

127 where \mathbf{u} denotes the vector of the control inputs, k is the current clock cycle, B is the input matrix that
 128 determines which state is affected by which input and in what measure, \mathbf{y} is the vector of outputs
 129 available for correction, and C is the output selection matrix. Next, we define some specific design
 130 constraints.

131 From the circuit side, we need to ensure that even if multiple states are mapped to the same
 132 register, the control input is the same. Note that in (4), the matrix B is an n_x -by- n_u matrix, where n_x
 133 is the number of states and n_u is the number of inputs. In this matrix, each element B_{ij} indicates the
 134 measure in which the input corresponding to the column j is applied to the state corresponding to the
 135 row i . If the same input is applied to several states, then the values corresponding to these states can
 136 all be set to the same value. Thus, we enforce that the same control (correction) input is applied to all
 137 the states corresponding to the same register by the appropriate choice of the values in the matrix B .

138 The control input $\mathbf{u}(k)$ is usually computed based on the outputs of the circuit and a given
 139 reference. Cost-wise the preferred solution is the simplest possible, mainly, a linear control law, i.e.,
 140 when the control input $\mathbf{u}(k)$ is computed as $\mathbf{u}(k) = -K\mathbf{y}(k)$, with K a constant matrix. The controller
 141 gain K is determined such that the closed-loop system – meaning that the control input is applied to
 142 the system described by (4) – is asymptotically stable. Thus, we have experimented with the control
 143 input computed as $\mathbf{u}(k) = -K(\mathbf{y}(k) - \mathbf{y}^d)$, where \mathbf{y}^d are the desired values. However, since model (4)
 144 is in most cases nonlinear, such a controller may not suffice, in which case nonlinear controllers can be
 145 designed.

146 The proposed methodology consists of the steps depicted in Figure 2. The inputs are: a register
 147 transfer level nominal digital design, a set of application specific constraints (e.g. the acceptable output
 148 error), and the aforementioned design specific constraints. The output is a CFLED model.

149 A final remark concerns the operands data representation, since it is an important implementation
 150 cost factor. Although in control engineering floating point is the preferred representation format, from
 151 the circuit design point of view, having fixed point operands is a major source of cost saving. Many
 152 designs are fine tuned to the application specific needs and use custom fixed point representation.
 153 Thus, if a fixed-point representation is chosen, the CFLED gains, as well as resulting states, cannot
 154 exceed the representation used for the initial implementation, and use fixed point representation as
 155 well.

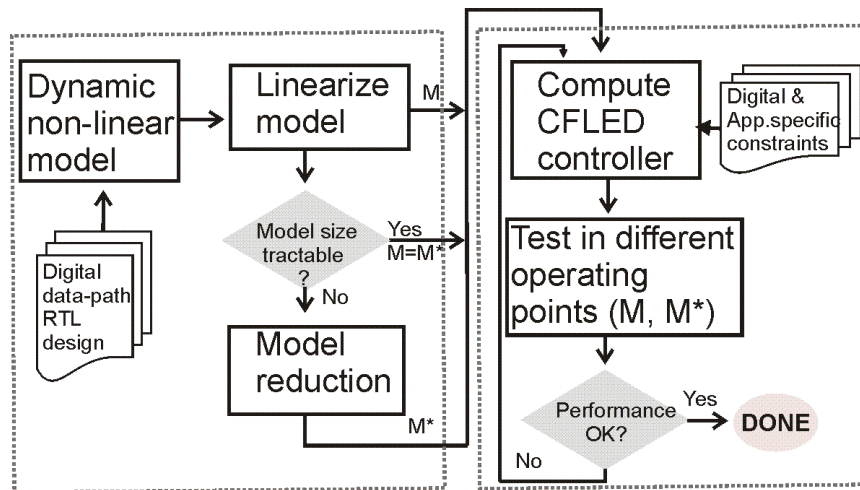


Figure 2. CFLED design steps

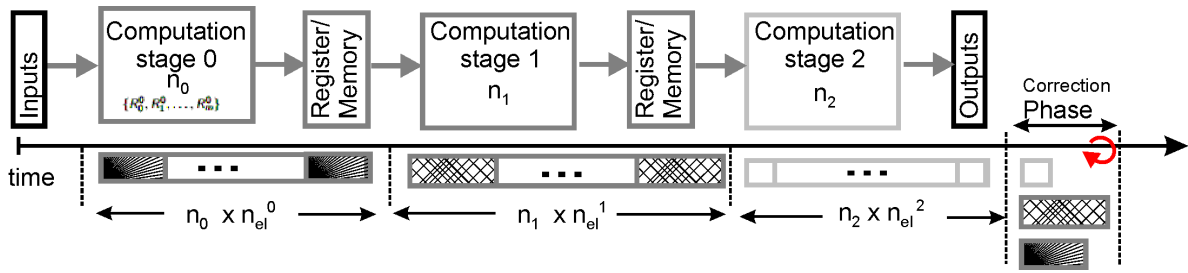


Figure 3. CFLED execution example. Three stages are considered in this example, each computing n_{el}^i results. Each result takes n_i cc for computation. First, the normal operation is performed. If, after finishing the computation, a difference is detected at the output, the correction operation is started. All three stages are executed – *rewinded* – in parallel with correction inputs added to designated registers.

156 2.3. Fault tolerant CFLED operation

157 Before describing the CFLED operation, we revise the circuit design constraints with respect to
 158 timing (*i.e.* number of clock cycles required computing a result). In digital circuit operation, a pipeline
 159 stage result is obtained at well defined moments in time (*i.e.* after a number of n_i clock cycles for
 160 an arbitrary processing stage i). In addition to this, we add the latency constraint that the CFLED
 161 enhanced circuit execution can not be larger than twice the execution of the nominal circuit. The latter
 162 implies that re-execution of an input data set is not applicable, otherwise we would be unable to justify
 163 the additional logic overhead with respect to time redundancy. However, given the principle of the
 164 correction loop, an extended execution, such that the correction offsets are added is required. This
 165 is handled in parallel for all the pipeline stages having non-zero coefficients in the K matrix, and we
 166 refer to it as pipeline stages execution rewind. Thus, latency increase is limited, and all computation
 167 sub-blocks are synchronized to the worst case number of clock-cycles it takes to compute a pipeline
 168 stage output result. This operating principle is depicted in Figure 3.

169 To summarize, the operation of the CFLED augmented digital circuit requires the following steps:

- 170 1. compute the difference between the output and the reference ($\mathbf{y}(k) - \mathbf{y}^d$),
- 171 2. determine the correction factors by means of $-K \times (\mathbf{y}(k) - \mathbf{y}^d)$,
- 172 3. rewind the computation by adding the obtained correction factors to the corresponding registers.

173 It should be emphasized that for a circuit composed of several sub-blocks, the rewinding process is
 174 performed only in the sub-modules for which the coefficients in K are non-zero. Furthermore, the
 175 re-executions is performed in parallel for the sub-blocks where the correction factors are applied –
 176 see Figure 3. Therefore, a correction phase duration is equal to the highest latency of the rewinded
 177 sub-modules. The correction process may take several phases/iterations, until the result is below the
 178 tolerated threshold.

179 A key issue is represented by the need of the \mathbf{y}^d reference. We solved this problem by employing
 180 two CFLED augmented processing pipeline, each providing the reference to the other circuit. In this
 181 case, an application specific filter may be employed, in order to exclude results that are out-of-bounds
 182 for the specific application.

183 3. Case Study - A Robot Arm Controller

184 3.1. Nominal circuit design

185 To illustrate the proposed approach, we consider the hardware implementation of a fuzzy
 186 controller for a two degree of freedom (2-DOF) robot arm. The parameters of the physical robot
 187 are described in [27], and the hardware implementation of the controller in [21]. The output of the
 188 nominal (controller) circuit implementation is the vector u (2 elements), that represents the inputs
 189 for controlling the robot arm. With x^{lr} (2 element vector) we denote the controller state, while x^r

190 represents the current state of the robot (4 element vector), and y^r is the reference that the robot arm
 191 should follow.

192 The hardware architecture is a fixed point implementation, using 24 bits operands, 8 bits for the
 193 integer part, and 16 bits for the fractional part. The equations and the numerical approximations used
 194 are described in [21]. For the purpose of this study, we focus on the register transfer level operations of
 195 the five pipelined processing blocks of the data-path depicted in Fig. 4:

- 196 1. Trigonometric function approximator, that computes the $\sin(x)$, $\sin(2x)$ and $\cos(x)$ - these three
 197 functions are evaluated based on the 2nd and 3rd order Taylor series, and are computed in
 198 parallel;
- 199 2. Computation of weighting functions - the computation of the three weighting functions h_1 , h_2 ,
 200 and v is serialized, with one element computed at a time;
- 201 3. Multiplication between the weighting functions - this block performs the 8 multiplications
 202 between h_1 or $(1 - h_1)$, h_2 or $1 - h_2$, and v or $(1 - v)$ sequentially;
- 203 4. Final gain matrix computation - this block performs the accumulation of 8 scalar-matrix products;
 204 the size of the matrices is 2×6 ; it employs a single multiply-add fused unit, and therefore, the 12
 205 elements of the final gain elements are computed sequentially;
- 206 5. Output computation - the output control vector is obtained by multiplication of the final gain
 207 matrix with the vector composed of the process state x^r and internal state x^{I^r} ; the two elements
 208 of the output vector are computed sequentially;

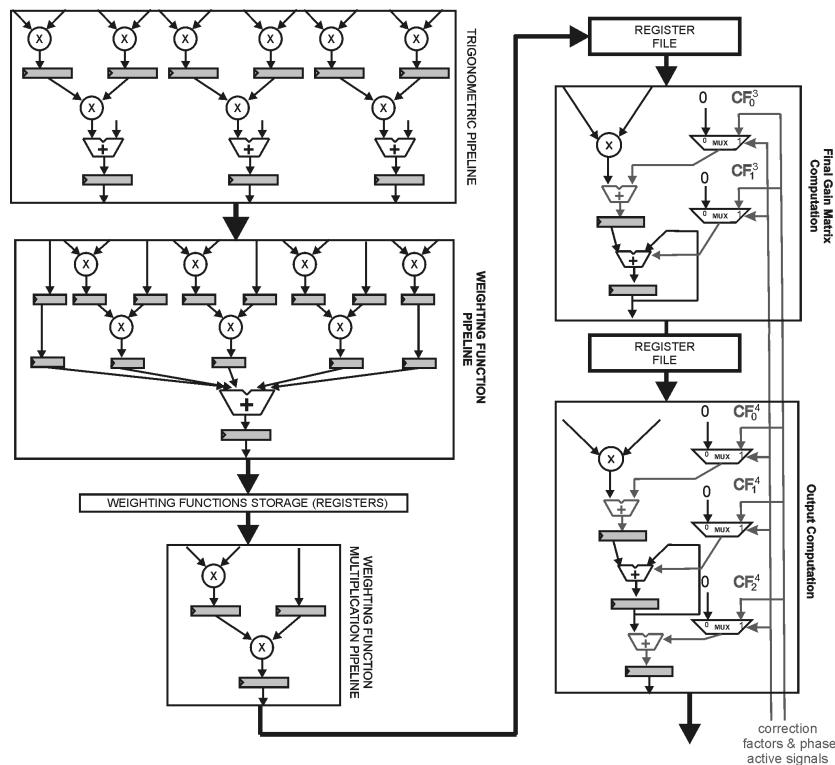


Figure 4. 2-DOF robot arm controller hardware architecture

209 The 2-DOF robot arm controller contains 34 data registers and the processing of a set of input
 210 samples requires 175 clock cycles.

211 3.2. Dynamic model and CFLED design

212 For the implemented architecture, a dynamic model has been developed, following the steps
 213 described in Section 2. The output of the system has been defined as the output of the circuit. The
 214 model is non-linear (consequence of the multiplication operation), of the form (4) and has 310 states.

215 In addition to the discussion from Section 2, in order to avoid obtaining a switching system or the need
 216 to include clock-dependence in the model, the blocks that compute results sequentially (e.g weighting
 217 functions, weighting function multiplication, and output computation) are modeled as parallel in the
 218 dynamic model.

219 For the actual design of the controller, we have opted to linearize the model in the zero equilibrium
 220 point, reduce it using a balanced realization, and compute the gain matrix by placing the closed-loop
 221 system poles as close as possible to the origin [28]. Because K is constant, it is computed offline. Finally,
 222 the resulting controller has been tested for the original nonlinear model. The correction gains are
 223 constant during the entire correction process and are independent of the fault rate affecting the circuit.
 224 The computed gains are multiplied by the difference between the actual and desired output vector
 225 ($\mathbf{u}[k] - \mathbf{u}^d[k]$), and their sum added at each clock cycle to the designated register during the correction
 226 operation phase. Furthermore, the vector \mathbf{u}^d is updated at the end of each correction phase execution.

227 Regarding the values in the gain matrix K , we have obtained values that are non-negligible for
 228 two out of five blocks: the final gain matrix computation and output computation blocks (5 registers
 229 out of 34). Thus, we employ CFLED for these two computational stages. The values for the gain factors
 230 corresponding to the two blocks are given in Table 1, where R_i^3 denotes registers within the final gain
 231 matrix computation block, while R_i^4 denotes registers within the output computation. During the
 232 correction phase, processing is performed only on these two blocks and the duration of the correction
 233 is given by the maximum of the latency of the two modules augmented with CFLED. Since the
 234 correction gain values are constant (computed offline), optimized implementation of multiplication
 235 with constants can be employed, using a simple shift-and-add approach.

236 First, the Matlab model of the CFLED enhanced 2-DOF controller with golden reference has
 237 been built. In the next step the golden reference has been replaced by a second CFLED controller
 238 that is also subject to probabilistic errors. A simple control unit determines if the difference between
 239 the outputs is smaller than the application specific error tolerance, chosen as 10^{-3} . If the computed
 240 output register difference is larger than this bound, the error correction phase is started. Thus, the fault
 241 tolerant solution relies on two CFLED enhanced models connected in reaction, that exchange data at
 242 the beginning of each correction phase.

243 We simulated the Matlab model to assess the performance of the overall system. The behavior
 244 of the proposed solution can be observed in Figure 5, which depicts outputs u_1 , and u_2 of the two
 245 controllers in the presence of errors. Note that the error at the output of one circuit influences the
 246 other. The simulation shows that up to cycle 27, the output of the two CFLED circuits are identical,
 247 thus, the black and red lines overlap. Then, the first controller has errors manifesting at the output u_1 ,
 248 thus, triggering the correction phase during the next simulation cycle. Due to the correction factors
 249 the two outputs influence each other, leading to a small perturbation in output u_2 , that is eliminated
 250 successfully during further correction phases. This is also the case for the other two errors that are
 251 larger in amplitude. The only difference is that the recovery time is larger. Given this observation,
 252 it makes sense to include a check in the control unit, that verifies if the output values are within the
 253 allowed range. For the considered use-case the range is $[-3.5, 3.5]$. If both CFLED enhanced circuits
 254 yield out of bounds results, then system failure occurs, and computation is restarted. Otherwise, they
 255 may serve as reference for each other during an error correction phase, if needed. If only one of the
 256 CFLED enhanced circuit outputs exceeds the range, then the other output is considered correct.

Table 1. CFLED K matrix values for registers in Fig. 4.

Input no.	Register	Gains \mathbf{u}	
1	R_1^3	-0.0011	-0.0038
2	R_0^3	0.0007	0.0024
3	R_1^4	-0.0017	-0.0022
4	R_0^4	-0.0103	-0.0092

257 3.3. Results and discussion

258 In this section, we discuss the results obtained by the proposed approach and compare them with
259 those obtained by a TMR.

260 3.3.1. Reliability analysis

261 The reliability analysis of the proposed approach has been performed using simulated fault
262 injection, in a Matlab-Modelsim co-simulation environment. Two main components are needed: the
263 Matlab model for the process, and the HDL CFLED RTL design simulated using Modelsim. The Matlab
264 simulation is responsible for generating and sending input data to the robot arm controller. It also
265 generates the correct output results, and handles the statistics recording and result post-processing.
266 The communication between the two CAD programs is through TCP/IP connection.

267 The simulated fault injection is performed in three phases:

- 268 I Setup: initializes all data structures from Matlab from the configuration files, loads the HDL
269 design inside the Modelsim environment with the parameters sent from Matlab, and generates a
270 TCL data structure in the HDL simulation environment that mirrors the Matlab simulated fault
271 injection configuration data (*i.e.* bit error probability, fault location).
- 272 II Simulation runs: One simulation step is run for both Matlab and Modelsim. In the Matlab
273 environment a set of input data and output gold values are computed. A TCL script with
274 appropriate command parameters is invoked through the TCP/IP connection. Next, the register
275 values for outputs, and the debug registers are read in Matlab, and data is logged in *.csv files.
- 276 III Results processing: Matlab scripts process the logged data and compute statistics.

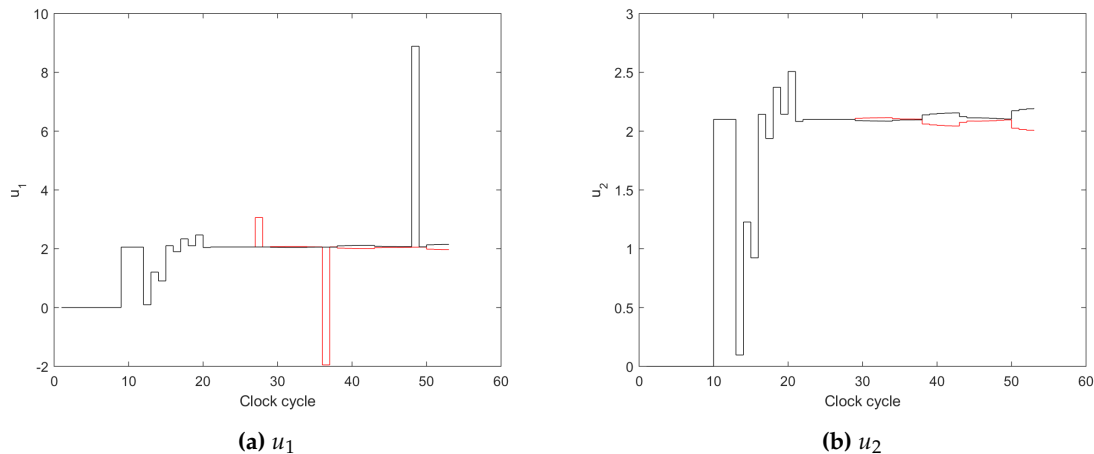


Figure 5. Matlab simulation example. Clock cycle accurate simulations of two CFLED enhanced 2-DOF units connected in reaction, and denoted with colours red and black, respectively.

277 We have performed the simulated fault injection both on the CFLED augmented architecture,
278 and on a fault tolerant controller that uses TMR. We have considered bit-flips that affect each flip-flop
279 within all data registers, with different fault rates per clock cycle: 10^{-4} , 10^{-5} , and 10^{-6} . During a
280 sample processing, for a bit-flip rate of 10^{-4} , the number of faults injected in the baseline architecture –
281 without any fault tolerant mechanism – is 14. For the fault tolerant designs – CFLED and TMR –, faults
282 have been applied for the entire design and during the entire execution.

283 We present the results in terms of:

- 284 1. Output failure rate - In this case, we have counted the number of outputs that have a difference
285 greater than 10^{-3} with respect to the correct output.

286 2. Gaussian distribution of the output error magnitude in terms of mean (μ) and covariance (σ) -
 287 This type of analysis has been performed because in arithmetic data-paths the error magnitude
 288 is in many cases more important than the number of errors (such as bit errors) affecting the
 289 result. Smaller values of the mean and of the covariance mean an improved distribution of error
 290 magnitude, and therefore, increased fault tolerance.

291 Results are depicted in Table 2 for the first component of the output vector (u_1), and Table 3 for
 292 the second component of the output vector (u_2). Although the TMR presents better output failure rate -
 293 a smaller number of erroneous frames -, the distribution of error magnitude is improved in the case of
 294 CFLED. This indicates that although the number of erroneous results is higher in the case of CFLED,
 295 the error magnitudes achieved with the proposed method is lower compared to TMR. Therefore, it
 296 can be noted that CFLED achieves its primary goal, to reduce or mitigate the magnitude of errors in
 297 arithmetic datapaths.

Table 2. Parameters of the Gaussian distributions and output failure rates for u_1^t

Bit error probability	Method	μ mean	σ covariance	Output failure rate
10^{-4}	CFLED	-0.1036	79.54	0.3202
	TMR	-0.5192	236.39	0.1516
10^{-5}	CFLED	-0.0043	0.4196	0.0186
	TMR	0.0277	1.3228	0.0066
10^{-6}	CFLED	-5.99×10^{-4}	1.3×10^{-3}	0.002
	TMR	-2.09×10^{-2}	2.826	0.0007

Table 3. Parameters of the Gaussian distributions and output failure rates for u_2^t

Bit error probability	Method	μ mean	σ covariance	Output failure rate
10^{-4}	CFLED	-0.0886	66.8871	0.3176
	TMR	0.10132	131.82	0.1436
10^{-5}	CFLED	-0.0334	3.6056	0.0229
	TMR	-0.0452	5.501	0.0039
10^{-6}	CFLED	0.0018	0.016	0.002
	TMR	0.0056	0.7344	0.0007

298 Figure 6 depicts the average number of correction phase executions, depending on the bit error
 299 probability. It can be noted that for a bit error probability of 10^{-6} , less than a quarter phase executions
 300 are required on average. Given that a phase execution requires 20 clock cycles - out of 175 clock cycles
 301 required for processing one sample -, less than 5 clock cycles are added on average to each sample
 302 processing. This means that the execution time is increased on average with less than 0.3%.

303 3.3.2. FPGA implementation results

304 The implementation results for the proposed CFLED enhanced 2-DOF controller design for Xilinx
 305 Virtex-7 VX485T-2 FPGA device, using the Xilinx Vivado 2017.1 tool are depicted in Table 4 for the
 306 baseline - non-fault tolerant - circuit, and the controlled, fault tolerant version, with two CFLED
 307 enhanced circuits providing the reference to the other.

308 FPGA implementation results indicate that the two circuit CFLED solution has an overhead of
 309 2.1x in terms of slices, with respect to the baseline circuit. In terms of DSP blocks, the CFLED solution
 310 contains the same number of blocks as two baseline circuits. Therefore, the CFLED solution uses 30%
 311 less slices with respect to the TMR, while having a third less DSP blocks. The results in Table 4 also
 312 indicate the low cost of the correction feedback with respect to the baseline circuit. Because this block

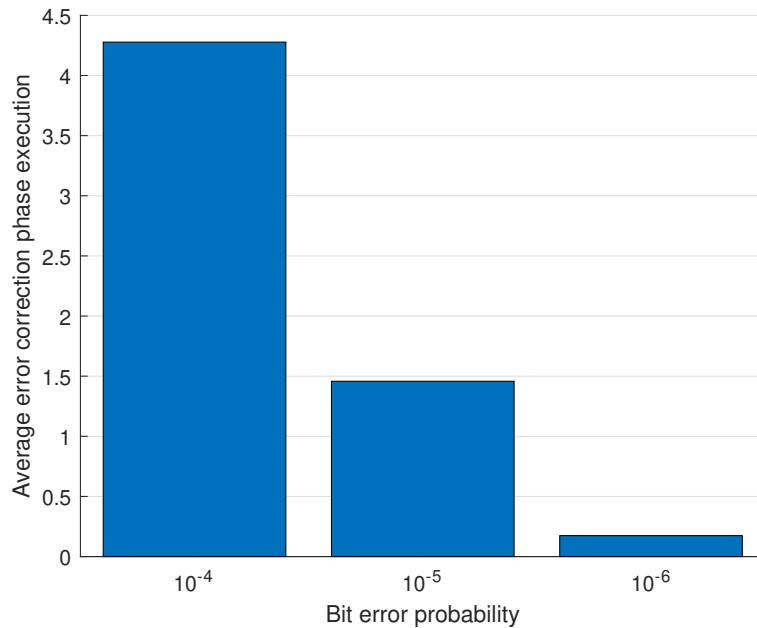


Figure 6. CFLED average phase execution increase for a maximum of 24 Correction Phase Executions.

Table 4. Implementation results

Design	Slices	DSP Blocks	Frequency [MHz]
Baseline	1948	34	142
TMR	5844	102	142
CFLED	4052	68	142

313 consists of 4 multipliers with constants – using a simple shift-and-add approach –, no dedicated DSP
 314 blocks are required, while the overhead in logic slices is rather negligible.

315 4. Conclusions

316 To the best of our knowledge, this paper represents the first attempt to improve the reliability
 317 of digital processing pipelines by employing control engineering techniques. CFLED requires
 318 the development of a dynamic model associated to the processing pipeline, and the design of a
 319 feedback controller that computes correction factors. The correction to be applied is computed as the
 320 multiplication between offline computed constants with the difference between the circuit’s output and
 321 the reference, and they are added to a sub-set of registers within the processing pipeline. A key issue
 322 is represented by obtaining the reference. In this paper, we propose to use two CFLED augmented
 323 data-paths, each providing the reference to the other.

324 Reliability estimates obtained by means of simulated fault injection for a hardware architecture
 325 of a two degree-of-freedom robotic arm controller indicates that the error magnitude of the CFLED
 326 augmented circuit is reduced with respect to a classic TMR based solution. Regarding the cost overhead
 327 for an FPGA based implementation, CFLED shows a 30% reduction in slice based resources compared
 328 to the TMR.

329 Thus, future work will consist of reducing the cost of this solution, by employing reduced
 330 precision replicas or approximate methods for part of the data-paths.

331 **Author Contributions:** “Conceptualization, O.B., A.A., Zs.L.; methodology, O.B, Zs.L.; software Matlab model,
 332 Zs.L.; HDL architecture O.B., A.A., validation, O.B., A.A.; investigation, O.B.,A.A., Zs.L.; writing–original
 333 draft preparation, O.B, A.A.; writing–review and editing, Zs.L.; visualization, O.B.; supervision, O.B.; project
 334 administration, O.B.; funding acquisition,O.B., A.A., Zs.L. All authors have read and agreed to the published

335 version of the manuscript.”, please turn to the [CRediT taxonomy](#) for the term explanation. Authorship must be
336 limited to those who have contributed substantially to the work reported.

337 **Funding:** “This research was funded by European Space Agency ITI REDOUBT activity.”

338 **Abbreviations**

339 The following abbreviations are used in this manuscript:

FPGA	Field Programmable Gate Array
TMR	Triple Modular Redundancy
ASIC	Application Specific Integrated Circuit
MRF	Markov Random Field
340 CFLED	Control Feedback Loop Error Decimation
DSP	Digital Signal Processing
HDL	Hardware Description Language
RTL	Register Transfer Level

341 **References**

- 342 1. von Neumann, J. Probabilistic Logics and the Synthesis of Reliable Organisms from Unreliable Components. *Automata Studies* **1956**, pp. 43–98.
- 343 2. Sánchez, A.; Entrena, L.; Kastensmidt, F. Approximate TMR for selective error mitigation in FPGAs based
344 on testability analysis. 2018 NASA/ESA Conference on Adaptive Hardware and Systems (AHS), 2018, pp.
345 112–119.
- 346 3. Sánchez-Clemente, A.J.; Entrena, L.; García-Valderas, M. Partial TMR in FPGAs Using Approximate Logic
347 Circuits. *IEEE Transactions on Nuclear Science* **2016**, *63*, 2233–2240.
- 348 4. Chen, K.; Han, J.; Lombardi, F. Two Approximate Voting Schemes for Reliable Computing. *IEEE*
349 *Transactions on Computers* **2017**, *66*, 1227–1239. doi:10.1109/TC.2017.2653780.
- 350 5. Chen, K.; Han, J.; Lombardi, F. Two Approximate Voting Schemes for Reliable Computing. *IEEE*
351 *Transactions on Computers* **2017**, *66*, 1227–1239.
- 352 6. Rodrigues, G.; Lima Kastensmidt, F.; Bosio, A. Survey on Approximate Computing and Its Intrinsic Fault
353 Tolerance. *Electronics* **2020**, *9*, 557. doi:10.3390/electronics9040557.
- 354 7. Huang, Y. High-Efficiency Soft-Error-Tolerant Digital Signal Processing Using Fine-Grain
355 Subword-Detection Processing. *IEEE Transactions on Very Large Scale Integration (VLSI) Systems* **2010**,
356 *18*, 291–304. doi:10.1109/TVLSI.2008.2009636.
- 357 8. Wali, I.; Casseau, E.; Tisserand, A. An efficient framework for design and assessment of arithmetic operators
358 with Reduced-Precision Redundancy. 2017 Conference on Design and Architectures for Signal and Image
359 Processing (DASIP), 2017, pp. 1–6.
- 360 9. Wey, I.; Peng, C.; Liao, F. Reliable Low-Power Multiplier Design Using Fixed-Width Replica
361 Redundancy Block. *IEEE Transactions on Very Large Scale Integration (VLSI) Systems* **2015**, *23*, 78–87.
362 doi:10.1109/TVLSI.2014.2303487.
- 363 10. Afzaal, U.; Lee, J. A Self-Checking TMR Voter for Increased Reliability Consensus Voting in FPGAs. *IEEE*
364 *Transactions on Nuclear Science* **2018**, *65*, 1133–1139.
- 365 11. Ló, T.B.; Kastensmidt, F.L.; Beck, A.C.S. Towards an adaptable bit-width NMR voter for multiple error
366 masking. 2014 IEEE International Symposium on Defect and Fault Tolerance in VLSI and Nanotechnology
367 Systems (DFT), 2014, pp. 258–263.
- 368 12. Arifeen, T.; Hassan, A.; Lee, J.A. A Fault Tolerant Voter for Approximate Triple Modular Redundancy.
369 *Electronics* **2019**, *8*, 332. doi:10.3390/electronics8030332.
- 370 13. Laurenciu, N.C.; Gupta, T.; Savin, V.; Cotofana, S.D. Error Correction Code protected Data Processing
371 Units. 2016 IEEE/ACM International Symposium on Nanoscale Architectures (NANOARCH), 2016, pp.
372 37–42.
- 373 14. Luan, Z.; Chen, X.; Ge, N.; Wang, Z. Simplified fault-tolerant FIR filter architecture based on redundant
374 residue number system. *Electronics Letters* **2014**, *50*, 1768–1770. doi:10.1049/el.2014.3508.
- 375

- 376 15. Chang, C.; Molahosseini, A.S.; Zarandi, A.A.E.; Tay, T.F. Residue Number Systems: A New Paradigm
377 to Datapath Optimization for Low-Power and High-Performance Digital Signal Processing Applications.
378 *IEEE Circuits and Systems Magazine* **2015**, *15*, 26–44.
- 379 16. Li, Y.; Li, Y.; Jie, H.; Hu, J.; Yang, F.; Zeng, X.; Cockburn, B.; Chen, J. Feedback-Based Low-Power
380 Soft-Error-Tolerant Design for Dual-Modular Redundancy. *IEEE Transactions on Very Large Scale Integration*
381 *(VLSI) Systems* **2018**, *26*, 1585–1589. doi:10.1109/TVLSI.2018.2819896.
- 382 17. Li, Y.; Li, Y.; Wey, I.; Hu, J.; Yang, F.; Zeng, X.; Jiang, X.; Chen, J. Low-Power Noise-Immune Nanoscale
383 Circuit Design Using Coding-Based Partial MRF Method. *IEEE Journal of Solid-State Circuits* **2018**,
384 *53*, 2389–2398.
- 385 18. Štefan Krištofík.; Baláž, M.; Malík, P. Hardware redundancy architecture based on reconfigurable
386 logic blocks with persistent high reliability improvement. *Microelectronics Reliability* **2018**, *86*, 38 – 53.
387 doi:https://doi.org/10.1016/j.microrel.2018.04.010.
- 388 19. Yang, J.; Kwak, S.W. Corrective control of parallel interconnected asynchronous sequential machines with
389 output feedback. *IET Control Theory Applications* **2019**, *13*, 693–701.
- 390 20. Yang, J.; Kwak, S.W. Model matching and fault-tolerant control of switched asynchronous sequential
391 machines with transient faults. *IET Control Theory Applications* **2019**, *13*, 1882–1890.
- 392 21. Boncalo, O.; Amaricai, A.; Lendek, Zs. Configurable Hardware Accelerator Architecture for Takagi-Sugeno
393 Fuzzy Controller. Proceedings of the Euromicro Conference on Digital System Design; , 2019; pp. 1–6.
- 394 22. Jamshidpour, E.; Poure, P.; Saadate, S. Photovoltaic Systems Reliability Improvement by Real-Time
395 FPGA-Based Switch Failure Diagnosis and Fault-Tolerant DC-DC Converter. *IEEE Transactions on Industrial*
396 *Electronics* **2015**, *62*, 7247–7255.
- 397 23. Cabal-Yepez, E.; Valtierra-Rodriguez, M.; Romero-Troncoso, R.J.; Garcia-Perez, A.; Osornio-Rios, R.A.;
398 Miranda-Vidales, H.; Alvarez-Salas, R. FPGA-based entropy neural processor for online detection of
399 multiple combined faults on induction motors. *Mechanical Systems and Signal Processing* **2012**, *30*, 123–130.
- 400 24. Karimi, S.; Poure, P.; Saadate, S. FPGA-based fully digital fast power switch fault detection and
401 compensation for three-phase shunt active filters. *Electric Power Systems Research* **2008**, *78*, 1933–1940.
- 402 25. Srebro, A. Fault-tolerant algorithm for a mobile robot solving a maze. *The Challenges of Modern Technology*
403 **2013**, *4*, 21–29.
- 404 26. Zhao, Z.; Wang, J.; Cao, J.; Gao, W.; Ren, Q. A Fault-tolerant Architecture for Mobile Robot Localization.
405 2019 IEEE 15th International Conference on Control and Automation (ICCA), 2019, pp. 584–589.
- 406 27. Lendek, Zs.; Nagy, Z.; Lauber, J. Local stabilization of discrete-time TS descriptor systems. *Engineering*
407 *Applications of Artificial Intelligence* **2018**, *67*, 409–418.
- 408 28. Levine, W.S. *The Control Systems Handbook, Second Edition: Control System Advanced Methods, Second Edition*,
409 2nd ed.; CRC Press, Inc.: USA, 2009.

410 **Sample Availability:** Samples of the compounds are available from the authors.

411 © 2020 by the authors. Submitted to *Electronics* for possible open access publication
412 under the terms and conditions of the Creative Commons Attribution (CC BY) license
413 (<http://creativecommons.org/licenses/by/4.0/>).